Anal. Bioanal. Electrochem., Vol. 10, No. 5, 2018, 594-611

Analytical & Bioanalytical Electrochemistry

2018 by CEE
www.abechem.com

Full Paper

Investigating Electrochemical Behavior of the Nugget Zone in Dissimilar Friction Stir Lap Welded of Copper–Brass Joints

Kamran Amini[1,*] and Farhad Gharavi[2]

[1]*Department of Mechanical Engineering, Tiran Branch, Islamic Azad University, Isfahan, Iran*
[2]*Department of Materials Engineering, Sirjan Branch, Islamic Azad University, Sirjan, Iran*

*Corresponding Author, Tel.: +989131651659
E-Mail: k_amini@iautiran.ac.ir

Received: 10 February 2018 / Received in revised form: 29 April 2018 / Accepted: 13 May 2018 / Published online: 31 May 2018

Abstract- In this study, the weld nugget zone (WNZ) electrochemical behavior in copper-brass plates, welded using friction stir lap welding, in 0.015 M borate-buffered(Borax) (pH 9.3) and 1 M NaCl (pH 7.2) solutions are investigated. Therefore, dissimilar copper/ brass plates welded with welding conditions of welding speed of 25 mm/min and rotation speed of 710 rpm. Features of specimen welded nugget zone under open circuit potential; potentiodynamic polarizations are compered and then the morphology of the products corrosion formed in polarization experiment are analyzed using SEM. Electrochemical impedance spectroscopy (EIS) is used for the characterization of surface films formed on the welded specimens during 3600s immersion at E_{ocp} in the two test solutions. Results showed that the welding process reduced the welded NZ corrosion resistance and offered lower corrosion resistance than copper and higher corrosion resistance than brass in 1 M NaCl (pH 7.2) solution. On the other hand, polarization plots showed that welding process results in current densities decreases from 0.512 for copper and 0.711 for brass to 0.213 μAcm^{-2} for the WNZ and significant shifts toward positive for corrosion potential in Borax solution. Indeed, the welded NZ corrosion rate in Borax solution was less than that in 1 M NaCl. The oxide film formed on the welded joints of NZ surface was more porous in borate buffer solution than in the NaCl solution. The hardness of welded joints was higher than copper and brass, and the highest hardness observed in the welded specimen nugget zone with low heat input during the welding process, because the grain refined most meaningfully in the welded joints NZ during welding process.

Keyword - Friction Stir Welding, Copper, Brass Alloy, Electrochemical Behavior

1. INTRODUCTION

Copper is the fifth most common metal in the earth's crust, and very valuable in pure or alloyed forms. Brass, bronze and nickel are the most significant copper alloys. Copper and its alloys are extensively used in industries due to its promising properties such as suitable corrosion resistance, high electrical and thermal conductivity, mechanical workability and malleability [1,2]. Copper and its alloys are extremely considered due to their wide applications in the production of wire, sheets and pipelines in electronic industries, power stations, marine industries, heat exchangers and cooling towers [3,4]. Copper is identified as a good new that provides suitable corrosion resistance in the atmosphere and some chemical environments due to the formation of a protective oxide film or a nonconductive layer of corrosion yields on its surface [5,6]. Brass has been generally used in power plant and shipboard condensers, and petrochemical heat exchangers [7,8]. Brass materials are quite new. If the zinc content grows in the alloy, α-phase changes to β-phase, and gets more prone to corrosion occurrence. However, it reacts simply in usual environments having oxygen. Brass dezincification is one of the famous and common processes by means of which brass misses its appropriate physical and mechanical properties resulting in structure failure [7]. Therefore, its corrosion inhibition study has attracted much attention. Copper-based materials are frequently voluntary or involuntary exposed to chloride solutions. However, Cu is sensitive to corrosion in chloride media [9-10]. Hence, the high concentration of Cl^- in seawater causes serious corrosion of copper, which has brought enormous economic losses and many potential safety problems to the applying of marine industry. Thus, the evaluating copper corrosion in chloride environments is a subject of practical significance and essential academic [11]. The Cu alloys good corrosion resistance in seawater is associated to the formation of a corrosion products protective film in the initial stages of exposure. It is usually thought that the film internal part is made of cuprous oxide (Cu_2O) with cupric oxide (CuO) in the outer part; and the film has metallic ions in common with hydroxides, chlorides and carbonates [8]. Though this film starts emerging during primary contact with oxygenated water, it takes several weeks until the film to be becomes completely protective. When the film completely develops and reaches a steady state, the corrosion amount is generally low.

Normally, copper passivation in the alkaline solutions is very interesting due to the scientific significance of this phenomenon. Copper passive behavior in the alkaline solutions has been examined for the protective characteristics of the passive films and the electrochemical production of copper oxide layers [8,12,13]. The characteristics of copper oxides are related to the films composition. These investigations showed that passive films depends on several variables such as pH, applied potential, aggressive anions and aerating conditions [13,14]. Certainly, this passive film forms an effective cover against the metal dissolution. In industrial processes, copper and brass immerse in concentrated alkaline solutions sometimes and these concentrated solutions can disturb the passivation phenomena.

Therefore, the electrochemical behavior and copper and brass passivation in the alkaline solutions requires being completely understood [12]. In fact, there are several industrial processes in which copper have to resist in high and medium concentrations of hydroxides solutions. It should be noted that these concentrated solutions could affect the passive behavior. Consequently, it is vital to pay attention to copper behavior in the alkaline solutions [12]. Many studies have previously explained the properties and mechanism of copper and its alloys passive film formation [14-18]. However, enough information about the pH effect on the semi conductive behavior of the formed passive film on brass alloys was not available.

Corrosion resistance of friction stir welded materials formed during welding at various zones are not similar, due to the obvious microstructure gradient caused by the storage heating effect and plastic deformation during FSW. Therefore, FSW effect on the corrosion behavior of copper and its alloys has received much less attention. The purpose of present study is to investigate FSW effect of on corrosion behavior of pure copper, brass and nugget zone of welded joint in both 0.015 M Borax and 1 M NaCl solutions using Tafel polarization and electrochemical impedance spectrometry (EIS) techniques. Furthermore, in order to investigate surface corroded samples after corrosion tests, a scanning electron microscopy (SEM) was used.

2. EXPERIMENTAL METHOD

In this study, pure copper and brass plates of 220 mm in length, 140 mm in width, and 5 mm in thickness were welded through friction stir lap welding (FSLW).

Table 1 chemical composition of the copper plate (mass %)

Element	Cu	Zn	Sn	Fe	Ni	Si	Ag	Sb
Min.	99.934	0.0005	0.0238	0.0002	0.0131	0.0003	0.0236	0.0001

Table 2 chemical composition of the brass plate (mass %)

Element	Cu	Zn	Sn	Fe	Ni	Si	Bi	Sb	P	Pb
Min.	62.43	37.21	<0.001	0.15	<0.001	<0.001	0.002	0.005	0.01	0.08

Table 3 Tool Size used in experiment

Length of pin (mm)	Diameter of pin (mm)	Diameter of shoulder (mm)	Pitch (mm)	Cone Angle (degree)
9.50	10.50	24	1.2	60

Tables 1 and 2 indicate pure copper (99.934) and brass plates chemical composition, respectively. Pure copper plate produced by cold rolling under DIN EN1652 standard condition, and the brass plates with DIN 17660 standard condition produced by hot rolling; then the plates were half hard-tempered. A tool, made of DIN 1.2344 hot working tool steel, was used whose geometry is given in Fig. 1. The key dimensions of welding tool are summarized in Table 3.

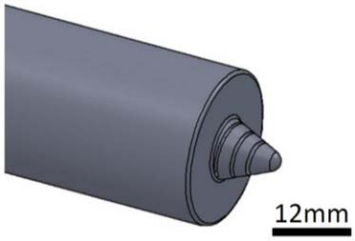

Fig. 1. shape of the welding tool designed in experiment

The welding tool was subjected to oil quenching and a three-stage tempering. Welding experiments were performed using an automatic CNC machine and the joint design was selected to produce lap welds. Fig. 2 shows the schematic representation of welding process and joint design. In the lap joint design, the brass and copper plates were put in Advancing and Retreating sides, respectively. This means that copper is located on top plate and Brass is located on bottom plate. The welding direction was normal to the plates rolling direction. During the FSLW, a 3° tilt angle and a plunge depth of 0.2 mm were applied to the tool. All welded samples are performed at welding speed of 25 mm/min and rotation speed of 710 rpm.

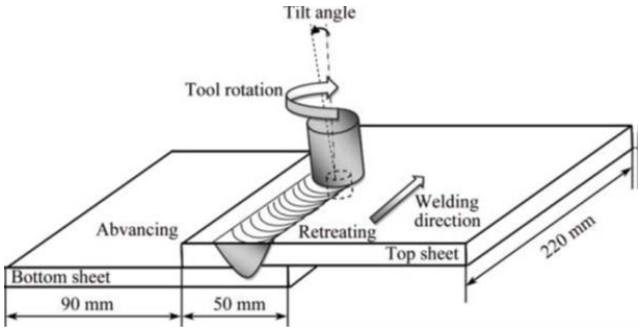

Fig. 2. Schematic of friction stir lap welding process and joint design used in this research

In order to investigate the corrosion behavior, a 10 mm×10 mm piece was cut from each specimen center part using sanding. After that, the grinding and degreasing operations were done and the specimens were washed by distilled water two times. After drying with air, all the electrochemical measurements were completed in a conventional three-electrode

electrochemical glass cell. The cell was opened to the air. The measurements were done at ambient temperature. The counter electrode was a graphite rod, whereas the reference electrode was a saturated calomel electrode (SCE). Electrochemical measurements were achieved using Ivium system controlled using a personal computer. Testing corrosion, 1 M NaCl (pH 7.2) and 0.015 M Borax (borate-buffered solution) (pH 9.3) solutions were used. Each specimen was immersed in these solutions for 3600s before performing any tests. After that, the Tafel polarization tests (with scanning rate of 1 mVs^{-1}) and EIS (in open circuit potential and frequency range of 100 kHz to 10 mHz with amplitude of 10 mV) were performed. Scanning electron microscopy (SEM) was used to analyze the surface of the samples after the corrosion tests. To achieve the necessary information about the welding process impact on the grain size, grain size was measured, and the image analysis of micrograph was performed. The grain size was obtained according to ASTM standard E112 [19] using linear intercept method. Microhardness measurement was performed using Shimadzu M micro-tester with a force of 200 g for 10 seconds at intervals of 1 mm according to ASTM E 384-05a standard [20] for both base metals (copper and brass) horizontally.

3. RESULTS AND DISCUSSION

3.1. Grain size and microhardness results

Fig. 3 illustrates average Vickers hardness distribution and grain size across the nugget zone (NZ) of welded joint, copper and brass sides. Based on Fig. 3, the hardness in the welded joints is higher than copper and brass, and the highest hardness is seen in the welded specimen nugget zone with low heat input during the welding process. Therefore, enhancing heat input causes an increase in the average grain size and a decrease in hardness at the welded joints nugget zone. It should be noted that the hardness value is carefully related to the grain size.

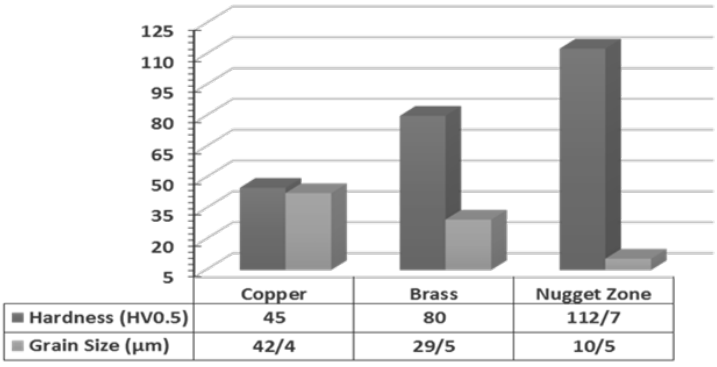

Fig. 3. variation of the average Vickers hardness distribution and grain size across the nugget zone (NZ) of welded joint

The grain refined most meaningfully in the welded joints NZ during welding process; thus, the NZ hardness is the highest. On the other hand, it is stated that the friction stir welding makes it easy to obtain a fine grain metal with high internal energy and a larger fraction of grain boundaries [21]. Furthermore, inside some grains and at grain boundaries, the residual stress and dislocation mass is high which Fattah-alhosseini and Imantalab [22] are documented similarly. Therefore, significant residual stress offers copper fine grain and its alloys with additional nuclei in order to produce much thicker passive film, which has an improvement in the corrosion resistance. In addition, the grain structures leads to fast passive film growth. In this regard, Imantalab and Fattah-alhosseini are reported the same results by study on electrochemical and passive behaviors of pure copper fabricated by accumulative roll-bonding (ARB) process [23].

3.2. Measurements of Open Circuit Potential

3.2.1. Diagrams of Potential–pH

Pourbaix diagram (diagram of potential–pH) offers a thermodynamic source to understand dissolution and oxide formation better in aqueous solutions at different electrochemical settings. Stability solid zones and the soluble types are explained in various events based on the standard of free energies. Potential E–pH diagrams for Cu and Zn in water with 1 M NaCl at the temperature of 25 °C is shown at Fig. 4. The thermodynamics information used to create Fig. 4 were acquired from the database compiled by Roine [24].

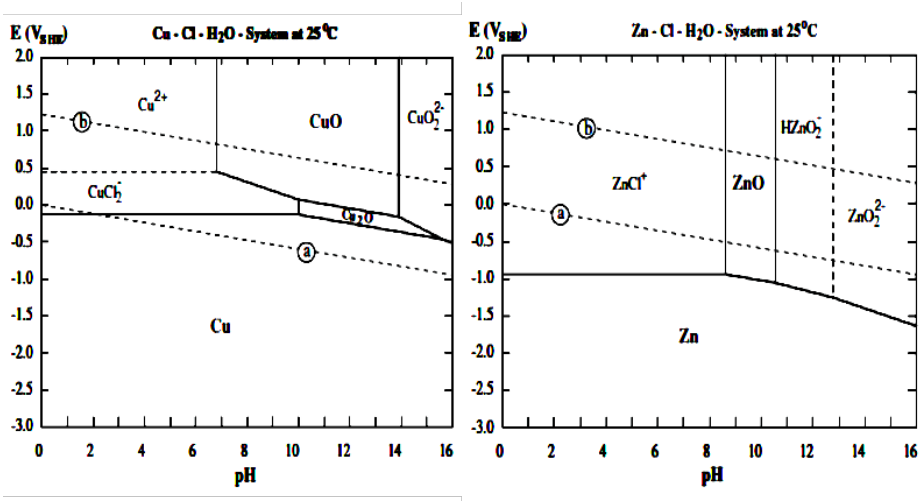

Fig. 4. Pourbaix diagrams of Cu and Zn in Cl^-–H_2O system at 25 degrees at 0.67 activity of Cl^-, equal to 1 M of NaCl [24]

3.2.2. Borate Buffer Solution (pH=9.3)

Fig. 5 shows E_{ocp} data measured for pure copper, brass alloy, and welded copper/brass nugget zone in the as-prepared borate buffer solution for the duration of 3600 s. The E_{ocp} curves for Cu specimen reduced among specimen immersion before the steady state occurrence. E_{ocp} decrease is a result of oxide film breakdown. After around 200 s, the E_{ocp} value becomes more positive, indicating the passive film formation and its effect on the productivity improvement with time passing [25]. Badawy et al. [26] reported the same discussion by research on Corrosion behavior of brass alloys in aqueous solutions of different pH. Furthermore, it is observed that the brass specimen OCP is directed toward positive values at the start of immersion. It is due to copper content enrichment on the surface of brass for its dezincification, which results in the potential enabling. According to Fig. 5, it is evident that a sharp growth in E_{ocp} was initially seen in the case of welded specimens followed by an increase in E_{ocp} to higher values than pure copper and brass. E_{ocp} increase is a result of rapid oxide film formation. On the other hand, after around 800s, E_{ocp} reaches steady state with time for welded specimen, which shows the passive film stability and its role in increasing productivity with time [25,26]. Therefore, the welded specimens thermodynamically suggest lesser tendencies to be corroded like pure copper and brass alloy.

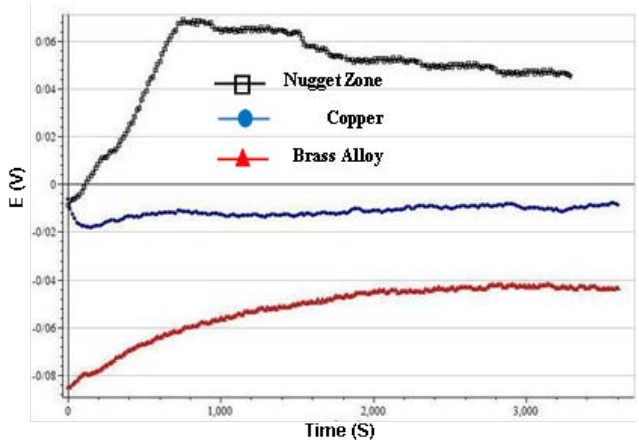

Fig. 5. Measurements of Cu open circuit, brass alloy and welded copper/brass nugget zone in 0.015 M Borax (pH 9.3) for 1 h

*3.2.3. Chloride Solution (*pH=7.2*)*

Fig. 6 displays E_{ocp} data measured for pure copper, brass and welded nugget zone by FSLW after immersion in the 1M as-prepared NaCl solution with pH of 7.2 for 3600 s. The E_{OCP} curves of Cu–Zn and Cu reduced among specimen immersion before the steady state occurrence. Great decrease in E_{OCP} was primarily evident in Cu and Cu–Zn and subsequently a steady state in E_{OCP} to a value higher to that for pure copper compared to brass metal. The

decrease in E_{OCP} is caused by oxide film failure, which exposes primary Cu–Zn surface. When the E_{OCP} reaches its lowest value, Zn starts to dissolve but Cu seems to be untouched resulting in Zn dealloying or de-zincification from Cu–Zn surface. The steady state E_{OCP} of Cu and the brass alloy slightly moved and happened after 1000 s. Alfantazi et al. [25] reported the same discussion by research on Corrosion behavior of copper alloys in chloride media. Although the E_{OCP} curve for welded specimen reduced among specimen immersion before the steady state occurrence, the welded nugget zone displays more positive potential than Cu and brass. The decrease in E_{OCP} is caused by oxide film breakdown, which is the same for the welded specimen. Zn dealloying showed similar trend to that of brass metal in some ways, as the curve for welded specimen. However, the welded specimens NZ offers much less tendency to Zn dealloying phenomena. Dealloying significantly depends on the dissimilarity between standard flexible potentials in atomic percentage composition, major fundamental elements, and kinetics of solid-state diffusion of the alloyed elements. Ateya and Pickering [27] report the same discussion by study on the effects of potential and kinetic parameters on the formation of passivating noble metal rich surface layers during the selective dissolution of binary alloys. The Cu–Zn and welded specimen dealloying happens in solutions from neutral to lower pH, due to the selective dissolution of Zn, according to E–pH diagrams of Fig. 4. Therefore, it can be said that welding process can change the welded specimen NZ microstructure and the microstructural aspects have significant effect on the strength of oxide film, which was formed on the welded specimen surface.

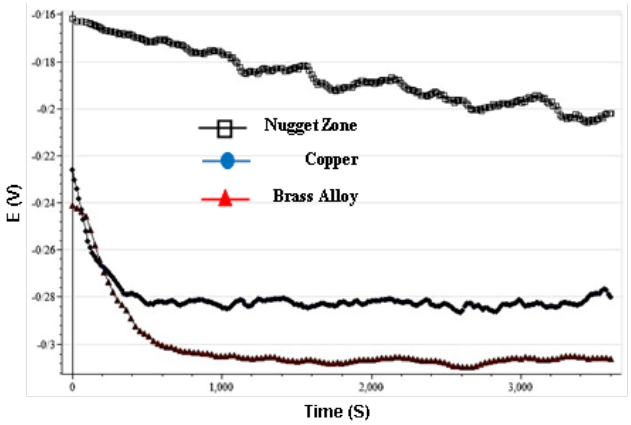

Fig. 6. Open circuit measurements for Cu, brass alloy and welded copper/brass nugget zone in 1 M NaCl (pH 7.2) for time duration of 1 h.

3.3. Polarization behavior with pH of 7.2

Fig. 7 shows the tested alloys polarization behavior obtained from NaCl solution with 7.2 pH. The open circuit potential (E_{OCP}) was -0.2 V_{SCE} for welded specimen, slightly higher than

the others were. Table 4 represents the corrosion potential (Ecorr), corrosion current density (I_{corr}), and corrosion rate (mpy). The corrosion current density (I_{corr}) was considered using cathodic branch Tafel extrapolation linear section with more than 95% accuracy for the past, which are more negative to E_{corr}, by 50 mV [28].

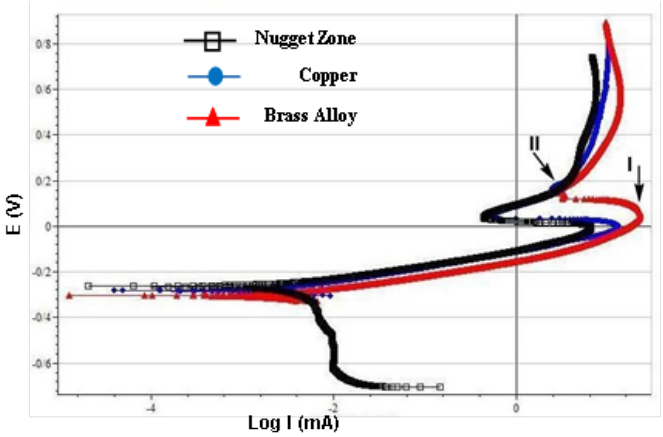

Fig. 7. Polarization behavior of Cu, brass alloy and welded copper/brass nugget zone in 1 M NaCl (pH 7.2). Arrows indicate I and II peaks positions

Table 4. The electrochemical data resulted from measurements of Cu, brass alloy and welded copper/brass nugget zone polarization in 1 M NaCl (pH 7.2)

Sample	**E_{corr} (V/SCE)**	**I_{corr} (μAcm^{-2})**	**C.R (mpy)**
Cu	-0.284	3.34	1.53
Brass	-0.303	6.76	3.11
Nugget Zone	-0.271	4.81	2.21

All of specimens' curves showed active behavior. Cu and welded specimen curves initiated with related active zone and subsequently the active–passive change occurring at similar potentials close to zero voltage *vs*. SCE (peak I)(Fig. 7). As E improved, one more peak (peak II) was seen at 0.15 V_{SCE} potential for brass followed by very limited range of passivity lasting for about 100 mV. The quick increase in the current is because of the film breakdown complemented by noticeable of working electrode corrosion. It appears that the Cu alloys polarization behavior in the mentioned solutions is controlled by the copper dissolution to soluble cuprous chloride ion complex ($CuCl_2$), according to E–pH diagram of Fig. 4. According to Table 4, it should be noted that the corrosion current density (I_{corr}) is not almost in the same direction as magnitude for all materials. Still, an I_{corr} minimum is observed for welded specimen and an I_{corr} maximum was seen for the brass alloy. Evidently,

performing welding process, the I_{corr} of the nugget zones is reduced due to the fundamental microstructural alterations occurring during the FSLW. This means that FSW increases the corrosion resistance of welded copper/brass.

Some researchers [29,30], have previously found that the polarization Tafel zone is not activation-controlled; it is a mass transport-kinetics process, where dissolution is controlled using the diffusion rate of $CuCl_2^-$ types from the electrode surface across a diffusion layer in which the gradient of concentration is calculated by the electrode potential. In this regard, Tromans and Sun [31] are reported the same discussion by work on Anodic polarization behavior of copper in aqueous chloride/ benzotriazole solutions.

3.4. Polarization behavior at pH 9.3

Cu polarization behavior, brass, and welded specimen in the buffered solution is shown in Fig. 8. Brass curve shows the active (Tafel) behavior zone where the reaction is supposed to be totally limited by charge transfer. A rapid increase of current with potential is observed in this zone, and both Zn and Cu are dissolved at the same time. While Zn dissolves in accordance with equation 1, the pourbaix diagram (Fig. 4) expects that Cu dissolve consistent with reaction 2 and 3 at moderate and high potentials, respectively [25]:

$$Zn \rightarrow Zn^{+2} + 2e^- \quad (1)$$

$$2Cu + H_2O \rightarrow Cu_2o + 2H^+ + 2e^- \quad (2)$$

$$Cu_2o + H_2O \rightarrow 2CuO + 2H^+ + 2e^- \quad (3)$$

The alloy behavior in this zone is intensely affected by the chloride ions presence.

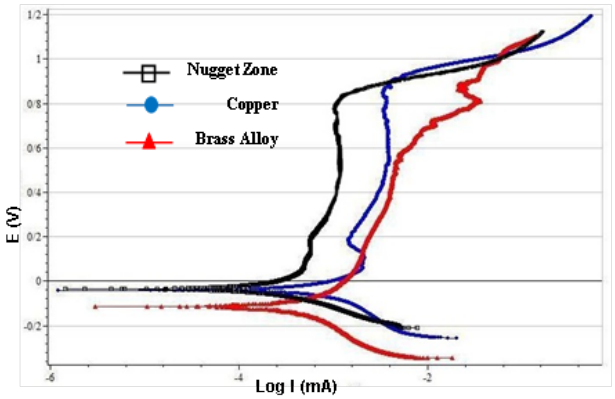

Fig. 8. Polarization behavior of Cu, brass alloy and welded copper/brass nugget zone in 0.015 M Borax (pH 9.3)

Table 5 represents the corrosion potential (Ecorr), corrosion current density (I_{corr}), and corrosion rate (mpy). In copper and welded specimen, passive peak I (Cu_2O) is seen at 0.15

V_{SCE}, which was higher than the outcomes in the NaCl solutions of Fig. 7. As E was highly anodic, the film breakdown was seen. The Cu outcomes were in accordance with those from Tromans and Sun [31]. FSW raised the E_b to somewhat greater potentials about the welded specimen. This increase shows the significance of pH control at the electrode surface close area. The dissimilarity in E_b can be explained by microstructure change during welding process.

Table 5. The electrochemical data resulted from measurements of Cu, brass alloy and welded copper/brass nugget zone polarization in 0.015 M Borax

Sample	E_{corr} (V/SCE)	I_{corr} (μAcm−2)	C.R (mpy)
Cu	-0.04	0.512	0.234
Brass	-0.17	0.711	0.321
Nugget Zone	-0.03	0.213	0.112

3.5. *EIS measurement (pH 7.2)*

Fig. 9 shows the Nyquist and Bode plots of Cu, brass, and the welded specimen at pH= 7.2 in 1 M NaCl solution, respectively. In Nyquist plots evaluation, the variance in actual impedance at frequencies of low and high is usually known as resistance of the charge transfer. The resistance of the charge transfer is related to metal and OHP (Outer Helmholtz Plane) resistance. All the resistances contribution is related to the interfaces of metal and solution; thus, items such as accumulation resistance, charge transfer resistance, diffusion layer resistance, film resistance, etc. are considered. Consequently, the polarization resistance (R_{pol}) in this study consists of the variance in actual impedance at frequencies of low and high [22,23].

All Nyquist plots show deficient semicircles. As shown in Fig. 9a, Nyquist plots have related behaviors and there are two time constants. It appears that the initial time constant has high frequencies, like an imperfect semi-circle and the latter is in the range of mid to low ones. Indeed, in Fig. 9, there was a decrease in the low frequency impedance with a growth in the heat input during welding process. According to the Nyquist plots, which show the two-time constant presence, the corresponding circuit model of Fig. 10 is for catching the best result. In the corresponding type, Q_p is the constant phase element of oxide film, R_p is the resistance of oxide film, Q_{dl} is the double layer constant phase element, R_{ct} is the charge-transfer resistance, and R_s is the solution resistance [22,23]. The modeling outcomes of this equivalent circuit indicate that there is an appropriate conformity between Nyquist plots and the modeled ones. Parameters obtained by fitting the Nyquist plots shown in Fig. 9 with the equivalent circuit shown in Fig. 10 are tabulated in Table 6.

Table 6. The electrochemical data resulted from measurements of Cu, brass alloy and welded copper/brass nugget zone impedance in 1 M NaCl (pH 7.2)

Sample	$R_{pass}\times10^3$ (ohm)	$R_{ct}\times10^3$ (ohm)	$R_{pol}\times10^3$ (ohm)
Cu	21.61	0.036	21.65
Brass	10.11	0.075	10.18
Nugget Zone	13.35	0.025	13.37

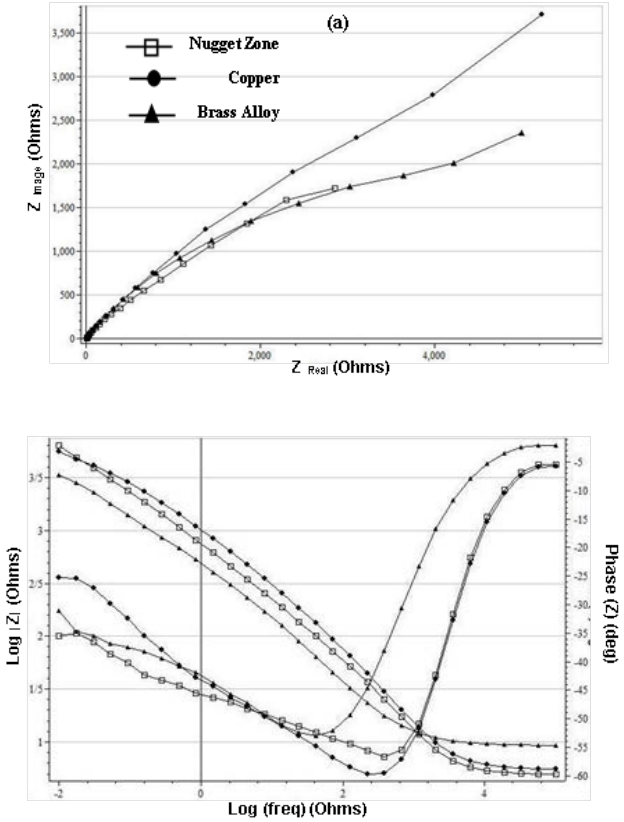

Fig. 9. (a) Nyquist plot (b) Bode plot for Cu, Brass alloy and welded copper/brass nugget zone in 1 M NaCl

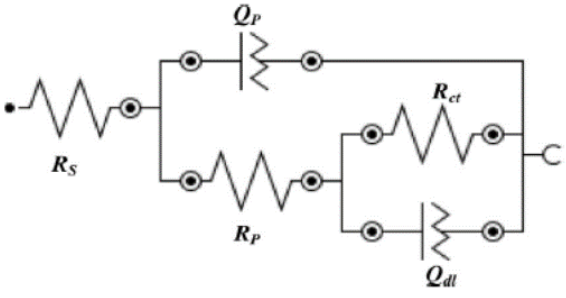

Fig. 10. The equivalent circuit utilized for the modeling of EIS data

Fig. 11 displays the disparity style of resistance of the polarization (=Rp+R_{ct}). As evident, the polarization resistance (R_{pol}) for copper specimen is the highest and the welded specimens have lower and higher values compared to copper and brass, respectively. This suggests that welded zone have a lower corrosion resistance than pure copper specimen. This zone has a lower tendency to the Zn dealloying than the brass alloy.

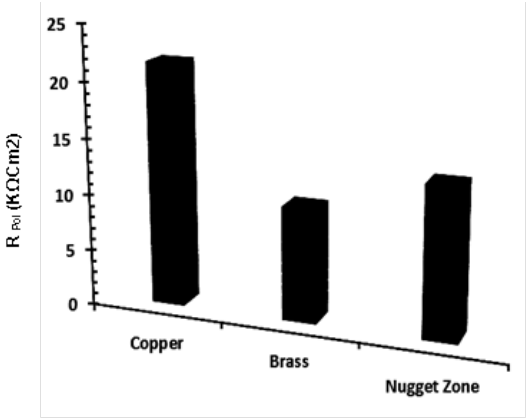

Fig. 11. The polarization resistance result from the modeling of experimental EIS data for Cu, brass alloy and welded copper/brass nugget zone in 1 M NaCl

According to Nyquist plot in Fig. 9a, the pure copper specimen has higher impedance than the others do, because the semicircle radios of Nyquist plot follow pure copper> welded zone> brass alloy in the similar solution. The low frequency impedance identifies the corrosion resistance. Hence, higher impedance value at low frequency displays better corrosion resistance. Therefore, the welded zone demonstrates lower and higher resistance compared to pure copper and brass alloy, respectively. According to Bode magnitude diagram (Fig. 9b), higher impedance obtained for pure copper specimen. This is in agreement with previous results from Nyquist curves, too. As known, the nobler electrochemical behavior is related to modulus of impedance |Z|. Although the Bode plots have not evidently permitted to accomplish the better electrochemical behavior for these studied specimens, the above-mentioned Nyquist plots state that pure copper specimen is better than the others are, as confirmed earlier. The obtained results from EIS calculations mention that the welded zone have lower and higher corrosion resistance than pure copper and brass, respectively. In this respect, the brass alloy has the lowest corrosion resistance.

3.6. EIS measurement at pH 9.3

Fig. 12 illustrates the Nyquist and Bode plots of pure copper, brass alloy and the welded specimens of NZ at OCP after immersion in borate buffer solution for 3600 s. During the evaluation of Nyquist plots, the difference in real impedance at lower and higher frequencies

is typically considered as a charge transfer resistance. The charge transfer resistance have to be in accordance to the resistance between metal and OHP (Outer Helmholtz Plane). The influence of all resistances is related to the metal/solution interface, which means that the charge transfer resistance, diffuse layer resistance, accumulation resistance, film resistance, etc. should be considered. Thus, in this study the difference in real impedance at lower and higher frequencies is measured as the polarization resistance (R_{pol}). According to Fig. 12a, Nyquist plots for pure copper and brass have related behaviors. In addition, two time constants are evident. It appears that the initial time constant has high frequencies, like an imperfect semi-circle and the latter is in the range of mid to low ones. Instead, the first semi-circle with high frequency is associated to the resistance of charge transfer and the resistance of diffuse layer. The semi-circle with low frequency is associated to the protective corrosion products surface film and other added types at the interface of metal and solution. It is stated that the formation of a passive layer on the Cu–Zn alloy in high pH solutions is composed of a composite group of phases of $ZnO{\cdot}xH_2O$ and Cu_2O/CuO [32]. Nevertheless, as seen in Fig. 12a, the welding process leads to a change in the impedance diagrams for both shape and size. This states that, the passive film feature is dissimilar in both welded specimens; and the corrosion mechanism could not be controlled similarly.

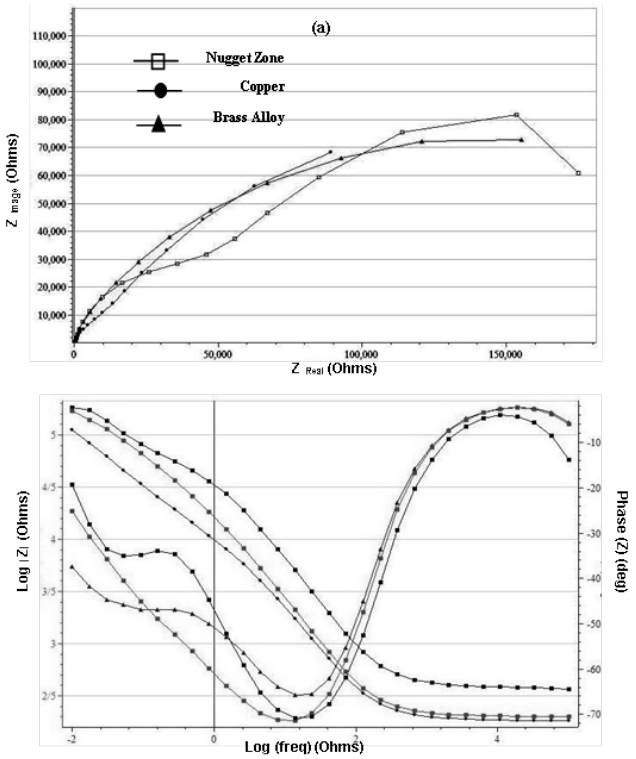

Fig. 12. The (a) Nyquist and (b) Bode plots of Cu, brass alloy and welded copper/brass nugget zone in 0.15 M Borax

The equivalent circuit shown in Fig. 13 was used to simulate the calculated impedance data on copper, brass and welded specimen in borate buffer solution. In this corresponding model, Q_p is the constant phase element of passive film, R_p is the passive film resistance, R_{ct} is the charge-transfer resistance, Q_{dl} is the double layer constant phase element, and R_s is the solution resistance.

Table 7. The electrochemical data resulted from measurements of Cu, brass alloy and welded copper/brass nugget zone impedance e in 0.015 M Borax

Sample	$R_{pass}\times10^3$ (ohm)	$R_{ct}\times10^3$ (ohm)	$R_{pol}\times10^3$ (ohm)
Cu	29.24	272.77	302.1
Brass	11.59	237.46	249.1
Nugget Zone	45.54	245.63	291.17

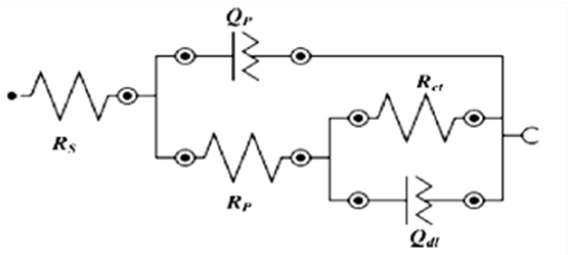

Fig. 13 .The equivalent circuit utilized for the modeling of EIS data

According to Table 7, the passive film resistance (R_p) and the charge-transfer resistance (R_{ct}) of welded specimen are higher than other specimens are. Unquestionably, the measured value of polarization resistance ($=R_p+R_{ct}$) of welded specimen is increased compared to the others. The corrosion current densities for welded specimen reduced more than the others did. These results are in accordance with the potentiodynamic polarization results. According to Bode magnitude diagram (Fig. 12b), higher impedance obtained for pure copper specimen. This is in agreement with previous results from Nyquist curves, too.

3.7. SEM analysis

After potentiodynamic polarization and the EIS tests in 1 M NaCl and 0.015 M Borax solutions, the WNZ specimens were subjected to SEM analysis. The corrosion occurrence always begins at restricted points at the surface and grows into a more general attack accompanied with the rich formation of corrosion products towards to the end of the polarization test. In the presence of NaCl solution, the corrosion products consist of pyramidal crystals on welded specimen (Fig. 14a).

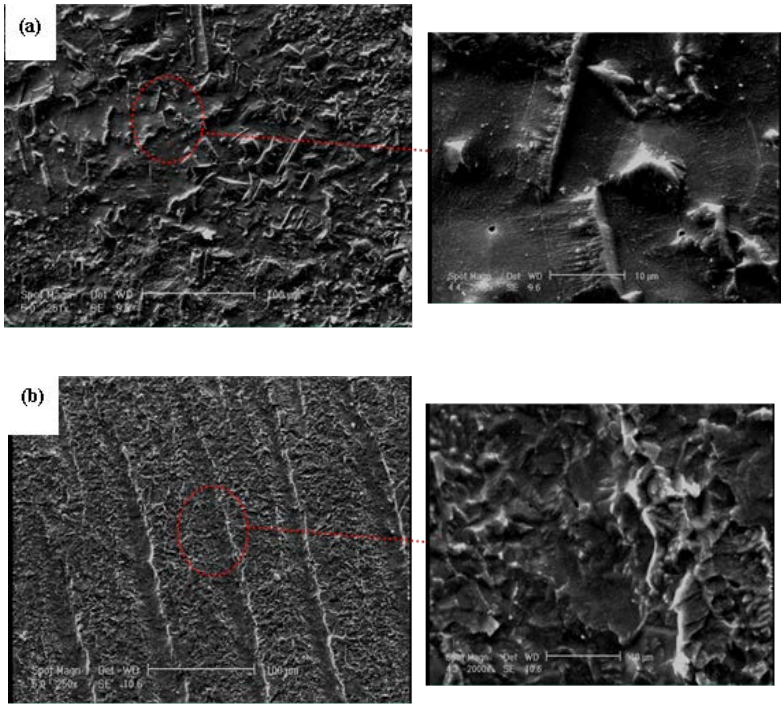

Fig. 14. SEM micrographs for the WNZ surfaces formed in solutions of various pH (a) pH 7.2 (b) pH 9.3

It seems that a rough layer of corrosion products protected the surface, which was a cuprous dichloride complex ($CuCl_2^-$) or cuprite (Cu_2O). Indeed, pit corrosion can be seen in a few spaces on the specimen surface, which is a local type of corrosion for copper and its alloys in NaCl solution. It is hard to state an exact composition from copper and its alloy surface in alkaline solution. Furthermore, it should be noted that the composition of formed surface layer rests on potential. Some studies [33,34] specified that a layer is on the brass surface in alkaline solution, which is generally ZnO at lower potentials. Thus, ZnO and Zn (OH_2) formed at more potentials that are negative while Cu_2O, CuO and Cu (OH_2) formation took place at higher potentials. The micrographs of the surface film formed in borax solution is displayed in Fig. 14b, where the entire surface was shielded with semi-pyramidal-like crystals containing Cu, Zn, O and OH, representing the presence of mixture of zinc-copper oxides or hydroxides. This film also was porous (i.e. few pit corrosion sites), like this for the NaCl solution specimen. However, it is higher protective than the film formed in NaCl solution. This results in a diffusion-control corrosion process [34,35].

4. CONCLUSION

Weld Nugget Zone electrochemical behavior in dissimilar Friction Stir Welded Lap Joints of Copper/Brass metals in NaCl and borate buffer solutions have been examined using open circuit potential, electrochemical impedance spectroscopy (EIS), potentio-dynamic

polarization curves, and surface morphology researches. The study conclusions are as follows:

1. In the NaCl solution, while the E_{OCP} curve for welded specimen reduced by specimen immersion earlier than the steady state happening, the welded NZ displays more positive potential than copper and brass. Still, in borate buffer solution, a sharp growth in E_{ocp} was firstly apparent in the case of welded specimen followed by an increase in E_{ocp} to higher than that for pure copper and brass. The increase in E_{ocp} is a result of rapid oxide film formation.
2. Tafel polarization curves presented that the nugget zone I_{corr} of welded joints is increased in NaCl solution, due to the intrinsic microstructural changes occurring throughout the welding process. Nevertheless, polarization plots in borate buffer solution indicated that welding process leads to current densities decrease and any important shift to positive for corrosion potentials.
3. In borate buffer solution, EIS results stated that higher heat input results in lesser polarization resistance in the welded nugget zone. However, the results from EIS measurements indicated that the polarization resistance for copper specimen is the highest value and the welded joints NZ had higher and lower values in NaCl solution compared to brass and copper, respectively.
4. The oxide film formed on the welded joints of NZ surface was more porous in borate buffer solution compared to the NaCl solution. This oxide film results in a diffusion-controlled corrosion process with less coverage in borate buffer solution.

REFERENCES

[1] M. A. Amin, and K. Khaled, Corros. Sci. 52 (2010) 1194.
[2] J. R. Davis, Copper and Copper Alloys. ASM International (2001).
[3] B. Duran, G. Bereket, and M. Duran, Prog. Org. Coat. 73 (2012) 162.
[4] E. S. M. Sherif, R. Erasmus, and J. Comins, J. coll. Inter. Sci. 306 (2007) 96.
[5] S. Adeloju, and H. Hughes, Corros. Sci. 26 (1986) 851.
[6] T. Suter, E. Moser, and H. Böhni, Corrs. Sci. 34 (1993) 1111.
[7] R. Ravichandran, and N. Rajendran, Appl. Surf. Sci. 239 (2005) 182.
[8] A. H. Tuthill, B. Todd, and J. Oldfield, Experience with Copper Alloy Tubing Water boxes and Piping in MSF Desalination Plants, Proceedings of world congress on desalination and water re-use, Madrid, Spain, 6-9 October (1997).
[9] M. Finšgar, Corrs. Sci. 72 (2013) 82.
[10] K. F. Khaled, Mater. Chem. Phys.125 (2011) 427.
[11] S. Hong, W. Chen, Y. Zhang, H. Q. Luo, M. Li, and N. B. Li, Corrs. Sci. 66 (2013) 308.
[12] A. Fattah-alhosseini, and S. Alizad, Anal. Bioanal. Electrochem. 7 (2015) 415.
[13] A. Fattah-alhosseini, and S. Alizad, Arab. J. Sci. Eng. 40 (2015) 2993.

[14] R. Procaccini, W. H. Schreiner, M. Vazquez, and S. Ceré, Appl. Surf. Sci. 268 (2013) 171.
[15] H. Wu, Y. Wang, Q. Zhong, M.S heng, H. Du, and Z. Li, J. Electroanal. Chem. 663 (2011) 59.
[16] M. Biton, G. Salitra, D. Aurbach, P. Mishkov, and D. Ilzycer, J. Electrochem. Soc. 153 (2006) B555.
[17] J. Kunze, V. Maurice, L. H. Klein, H. H. Strehblow, and P. Marcus, Corros. Sci. 46, 245 (2004)
[18] T. K. Mikic, I. Milosev, and B. Pihlar, J. Appl. Electrochem. 35 (2005) 975.
[19] ASTM Standard E112: Standard Test Methods for Determining Average Grain Size. West Conshohocken, ASTM International (2013). Doi: 10.1520/E0112
[20] ASTM Standard E384: Standard Test Method for Knoop and Vickers Hardness of Materials. West Conshohocken, ASTM International (2011). Doi: 10.1520/E0384-16
[21] H. Sarlak, M. Atapour, and M. Esmailzadeh, Mater. Des. 66 (2015) 209.
[22] A. Fattah-alhosseini, and O. Imantalab, J. Alloys Compd. 632 (2015) 48.
[23] O. Imantalab, and A. Fattah-alhosseini, J. Mater. Eng. Perform. 24 (2015) 2579.
[24] A. Roine, Outokumpu HSC chemistry for windows (Version 4.0), Outokumpu Research Oy, Pori, Finland, (2000).
[25] A. M. Alfantazi, T. M. Ahmed, and D. Tromans, Mater. Des. 30 (2009) 2425.
[26] W. A. Badawy, and F. M. Al-Kharafi, Corrosion 55 (1999) 268.
[27] B.G. Ateya, H.W. Pickering, Corros. Sci. 38(8), 1245 (1996)
[28] G. T. Burstein, Corros. Sci 47 (2005) 2858.
[29] A. L. Bacarella, and J. C. Griesss, J. Electrochem. Soci. 120 (1973) 459.
[30] D. Tromans, and J. C. Silva, Corrosion 53 (1997) 171.
[31] D. Tromans, and R. Sun, J. Electrochem. Soci. 138 (1991) 3235.
[32] G. Kılıncceker, and M. Erbil, Mater. Chem. Phys.119 (2010) 30.
[33] C. Liu, Q. Bi, A. Leyland, and A. Matthews, Corros. Sci. 45 (2003) 1243.
[34] M. M. Antonijevic, G. D. Bogdanovic, M. B. Radovanovic, M. B. Petrovic, and A. T. Stamenkovic, Int. J. Electrochem. Sci. 4 (2009) 654.